AJNR

Detailed MR Imaging Anatomy of the Cisternal Segments of the Glossopharyngeal, Vagus, and Spinal Accessory Nerves in the Posterior Fossa: The Use of 3D Balanced Fast-Field Echo MR Imaging

W.-J. Moon, H.G. Roh and E.C. Chung

AJNR Am J Neuroradiol 2009, 30 (6) 1116-1120
doi: https://doi.org/10.3174/ajnr.A1525
http://www.ajnr.org/content/30/6/1116

ORIGINAL RESEARCH

Detailed MR Imaging Anatomy of the Cisternal Segments of the Glossopharyngeal, Vagus, and Spinal Accessory Nerves in the Posterior Fossa: The Use of 3D Balanced Fast-Field Echo MR Imaging

W.-J. Moon
H.G. Roh
E.C. Chung

BACKGROUND AND PURPOSE: The cisternal segments of the lower cranial nerves (CNs) adjacent to the jugular foramen (JF) are difficult to identify reliably by routine MR imaging. We performed a 3D balanced fast-field echo imaging technique (3D-bFFE) to obtain detailed anatomy of the cisternal segments of CNs IX, X, and XI.

MATERIALS AND METHODS: 3D-bFFE was used to image the cisternal segments of the lower CNs in 20 healthy volunteers. As an anatomic landmark, CSF recesses adjacent to the JF were divided into 3 parts: the recess for the cochlear aqueduct, the recess for CN IX, and the recess for the CN X/XI complex. MR images were evaluated to identify the cisternal segment of each cranial nerve in relation to these anatomic landmarks.

RESULTS: The mean angles of the recess for the cochlear aqueduct for CN IX and CN X/XI to the posterior petrous bone were 41.6 ± 2.5°, 69.7 ± 3.1°, and 76.0 ± 3.4°, respectively ($P < .01$). The mean length of the recess for the cochlear aqueduct for CN IX and the CN X/XI complex was 5.91 ± 0.19, 5.08 ± 0.11, and 4.76 ± 0.13 cm, respectively ($P < .01$). 3D-bFFE adequately depicted the cisternal segments of CN IX on 38 sides (95%) and the CN X/XI complex on 39 sides (97.5%).

CONCLUSIONS: The cisternal segments of CN IX, CN X, and CN XI are well identified by using 3D-bFFE, especially by determining the angles of the CSF recesses adjacent to the JF.

With the advent of high-resolution MR imaging, the lower cranial nerves from the brain stem to the jugular foramen (JF) have been of concern to radiologists because the nerves have important roles for swallowing and parasympathetic function. The JF contains the glossopharyngeal nerve, vagus nerve, and spinal accessory nerves. Although more attention has been given to the facial nerve and vestibulocochlear nerves that pass through the internal acoustic canal, the lower cranial nerves that pass through the JF are also involved in various disease entities such as neurogenic tumors, glomus tumors, leptomeningeal disease (inflammatory and metastatic diseases), meningiomas, and neurovascular compression.[1,2]

With the use of current state-of-the-art imaging techniques, cranial nerves (CNs) IX, X, and XI can be depicted like the other CNs. However, routine MR imaging sequences are not always successful for visualizing the lower cranial nerves.[3-7] Incomplete visualization of these nerves is partly due to their close proximity and partly due to the lower resolution power of previous MR imaging sequences.[5] Unlike the facial nerve or vestibulocochlear nerves, the course of the lower CNs through the JF has not been well elucidated in vivo.[2,8] Sometimes, the JF and adjacent cochlear aqueduct cannot be easily identified on axial plane images.[1]

Regarding visualization of the CNs, especially within the cisternal spaces, a 3D constructive interference in steady state sequence, a 3D driven equilibrium sequence, a 3D fast imaging employing steady-state acquisition (FIESTA) sequence, and a gadolinium-enhanced 3D FIESTA sequence have been used successfully to demonstrate the presence of CNs within the cisternal spaces.[3, 5-7, 9]

The 3D balanced fast-field echo (3D-bFFE) sequence is a type of steady-state coherent MR imaging that has been used recently for the visualization of inner ear structures.[9,10] With a very short TR and complete balancing of the gradients in all 3 directions, 3D-bFFE produces high-spatial-resolution MR images with a high signal-intensity-to-noise ratio and a high contrast-to-noise ratio by being able to highlight signals from the CSF.[9] MR cisternography using the bFFE sequence effectively visualizes the neurovascular structures within the cerebellopontine angle cistern without CSF pulsation artifacts in a short examination time.[9]

We have proposed that we could easily identify the cisternal segments of the lower CNs if we were able to determine the level of the lower CNs that pass through the cisternal spaces. The level could be inferred by knowledge of the exact location and detailed anatomy of the CSF recesses adjacent to the JF that contain the lower CNs.

The purpose of this study was to define the detailed anatomy of the cisternal segments of the glossopharyngeal nerves and other nerves in conjunction with the CSF recesses adjacent

Received July 10, 2008; accepted after revision December 28.

From the Department of Radiology (W.-J.M., H.G.R.), Konkuk University Medical Center, Konkuk University School of Medicine, Korea; and Department of Radiology (E.C.C.), Kangbuk Samsung Hospital, Sungkyunkwan University School of Medicine, Seoul, Korea.

Paper previously presented as a scientific poster at: Annual Meeting of the American Society of Neuroradiology, May 6–12, 2006; San Diego, Calif.

Please address correspondence to Won-Jin Moon, MD, Department of Radiology, Konkuk University Medical Center, Konkuk University School of Medicine, Korea; e-mail: mdmoonwj@naver.com

DOI 10.3174/ajnr.A1525

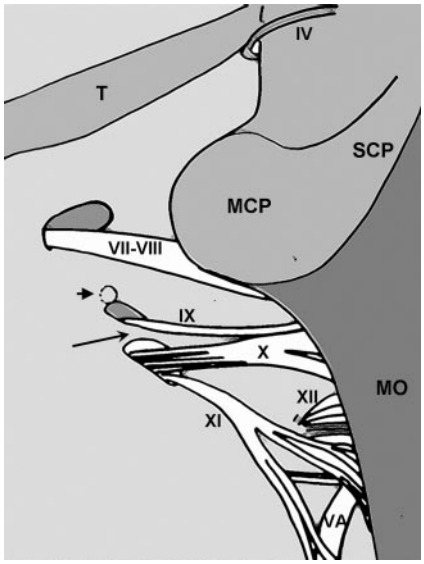

Fig 1. A diagrammatic representation of the posterior view of the left internal acoustic meatus and the JF after removal of the cerebellum. The short arrow indicates the opening of the cochlear aqueduct. The long arrow indicates the dural ring, which divides the endocranial openining of the JF: the recess for CN IX and the recess for CN X/XI. T indicates tentorium cerebelli; SCP, superior cerebellar peduncle; MCP, middle cerebellar peduncle; MO, medulla oblongata; VA, vertebral artery; IV, trochlear nerve; VII, facial nerve; VIII, vestibulocochlear nerve; IX, glossopharyngeal nerve; X, vagus nerve; XI, spinal accessory nerve; XII, hypoglossal nerve.

to the JF as depicted in 3D-bFFE MR images in healthy volunteer subjects. Special emphasis was placed on determination of the angles (the angles of the CSF recesses) to the adjacent petrous bone and the relationship of each recess to the adjacent structures.

Materials and Methods

Subjects

Twenty healthy volunteer subjects (8 men and 12 women) with an age range from 21 to 55 years (mean age, 35 years) were included in this study. Informed consent was obtained before the beginning of the study. Our internal institutional review board approved the study protocol.

MR Imaging Sequences

All MR imaging studies were conducted by using a 1.5T MR imaging system (Intera; Philips Medical Systems, Best, the Netherlands). MR cisternographic imaging was performed by using a 3D-bFFE sequence. The parameters for acquiring bFFE data were the following: TR, 7.95 ms; TE, 3.98 ms; FOV, 150 × 150 mm; flip angle, 50°; matrix, 256 × 256; section thickness, 0.7 mm (pixel size, 0.59 × 0.59 × 0.70 mm); acquisition time, 1 minute 33 seconds. MR imaging was performed in the axial plane by using a 6-channel sensitivity encoding (SENSE) head coil. All sequences were acquired by using SENSE with a SENSE factor of 2.

Image Analysis

Two neuroradiologists reviewed the 3D-bFFE images, and in case of disagreement, decisions were made by consensus.

In addition to the original axial raw data, the dataset of each 3D-bFFE sequence was reformatted in the oblique sagittal and coronal planes with a section thickness of 0.7 mm, perpendicular and parallel to the course of the evaluated nerve. Each image was analyzed by the use of a cross-link technique in which the position of 1 point in 1 plane can be easily correlated with the corresponding position of the same point in the other 2 orthogonal planes.

We analyzed each side of each subject to identify the CSF recesses adjacent to the JF (the recess for the cochlear aqueduct, the recess for CN IX, and the recess for the CN X/XI complex), and we analyzed each side of each subject to identify the 3 individual CNs in the cisternal space (Fig 1). We measured the angle of each CSF recess relative to the posterior surface of the petrous bone and the length of each CSF recess adjacent to the JF.

The anatomic visibility of the nerves was scored as excellent, fair, or poor. A score of 1 (poor) was assigned in cases in which the anatomic structure was not visible. A score of 2 (fair) was assigned in cases in which the anatomic structure was visible with fair image quality. A score of 3 (excellent) was assigned in cases in which the anatomic structure was clearly visible with an excellent image quality. For further identification of the individual nerves of the CN X/XI complex within the cisternal space, visibility was evaluated on oblique sagittal and coronal plane images and on axial plane images.

Statistical Analysis

Statistical analysis was performed by using the Statistical Package for the Social Sciences software (Version 12.0 for Windows; SPSS, Chicago, Ill). Data were tested for normality, and a paired *t* test was performed for comparison of the mean angle and length of each CSF recess. The Wilcoxon signed rank test was used for comparison of the visibility of the anatomic structures.

Results

The mean angle of each compartment relative to the posterior petrosal surface was 41.6 ± 2.5° for the recess of the cochlear aqueduct, 69.7 ± 3.1° for the recess of CN IX, and 76.0 ± 3.4° for the recess of CN X/XI ($P < .01$) (Fig 2).

The mean length of each compartment was 5.91 ± 0.19 cm for the recess of the cochlear aqueduct, 5.08 ± 0.11 cm for the recess of CN IX, and 4.76 ± 0.13 cm for the recess of CN X/XI ($P < .01$).

Visualization of the cisternal segments of CN IX and the CN X/XI complex was not significantly different on the 3D-bFFE sequence ($P = .180$). For CN IX, visualization was excellent in 34 of 40 sides (85%), fair for 4 sides (10%), and poor for 2 sides (5%). For CN X/XI, visualization was excellent in 30 of 40 sides (75%), fair for 9 sides (22.5%), and poor for only 1 side (2.5%) (Fig 3).

Regarding identification of each cisternal segment of the CN X/XI complex on oblique sagittal and coronal reformatted images, CN X could be easily seen separately from CN XI in 10 of 40 sides (25%) and could not be easily seen in 30 of 40 sides (75%) (Fig 4).

Discussion

Traditionally, the endocranial entrance of the JF has been divided into 2 compartments by the dural band: the smaller anterior part (pars nervosa) and the larger posterior part (pars venosa).[1,2,8] Although the glossopharyngeal nerve is located within the anterior part, the vagus and accessory nerves are located within the posterior part. Sometimes, there is a complete division of the foramen by a bony septum; partitions of the foramen vary in radiologic and anatomic studies.[1,11-14] Although there is variability in partitioning of the endocranial

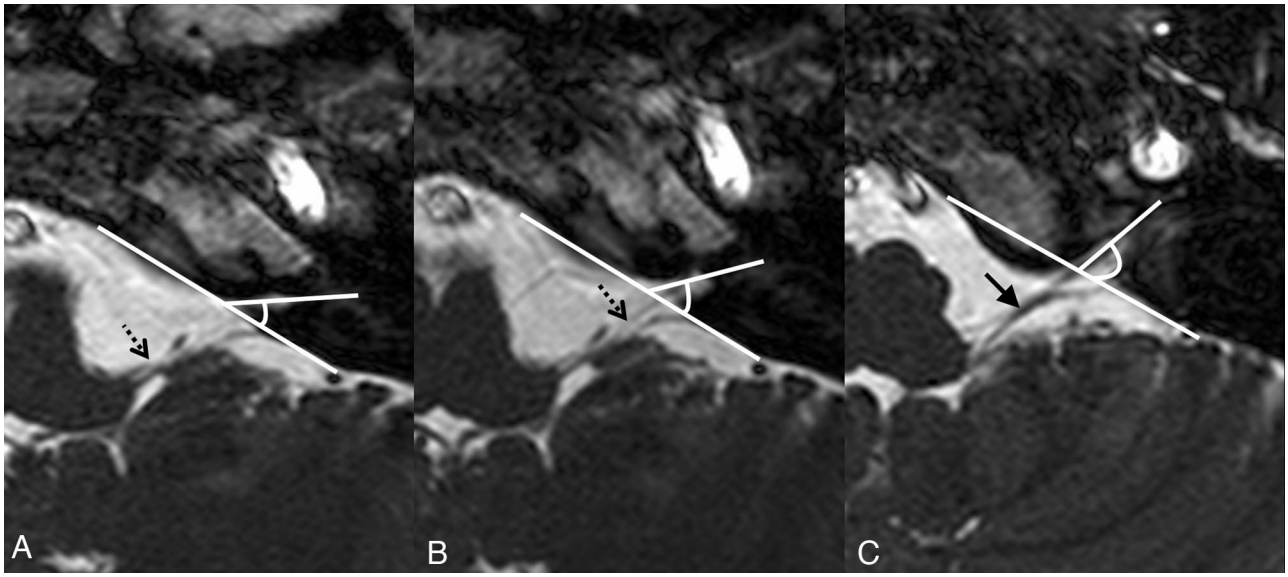

Fig 2. Axial 3D-bFFE images at the level of each compartment of the JF on the left side. The angle between each compartment and the posterior petrosal surface was visualized by a line drawing. *A–C,* The dotted arrow indicates CN IX (*A* and *B*) and the black arrow indicates the CN X/XI complex (*C*). Note that the angle of the cochlear aqueduct (*A*) is the smallest, whereas the angle of the recess for the CN X/XI complex (*C*) is the largest. The angle of the recess for CN IX (*B*) is between the angles of the cochlear aqueduct and the recess for the CN X/XI complex.

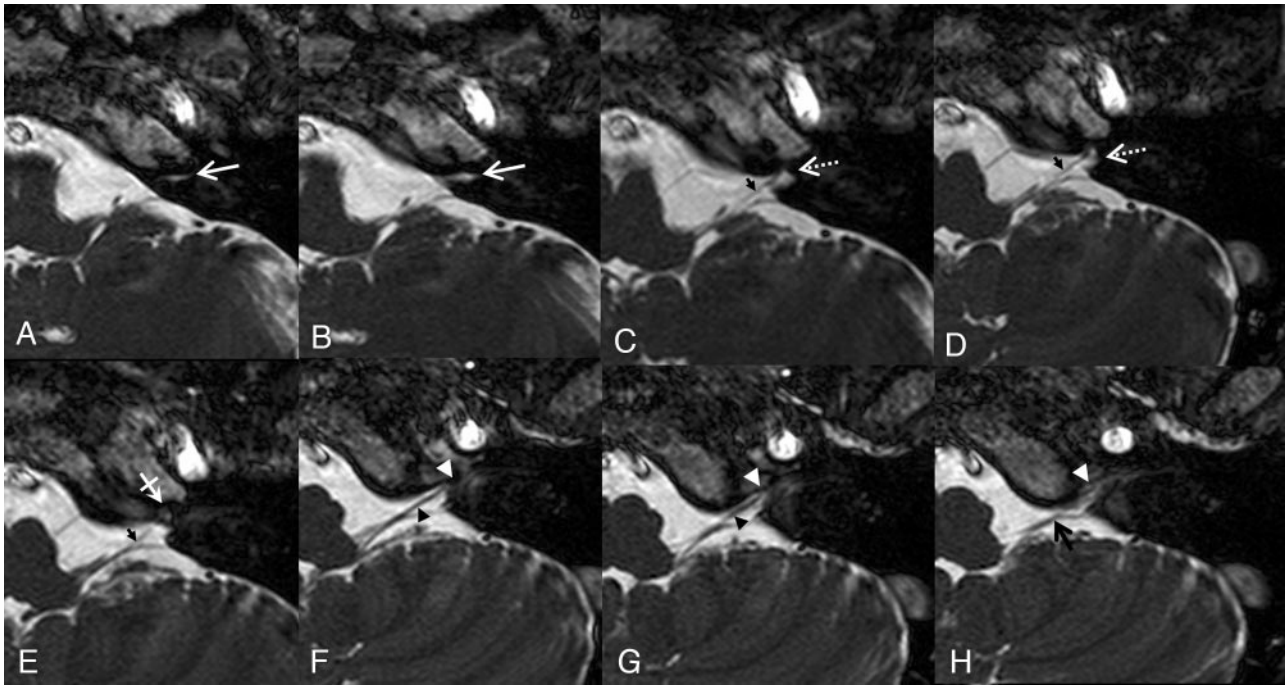

Fig 3. Axial 3D-bFFE images of the lower cranial nerves from the level of the cochlear aqueduct to the level of the lower margin of the JF on the left side. *A* and *B,* The white arrows indicate the recess for the cochlear aqueduct. *C–E,* Just below the level of the cochlear aqueduct, the glossopharyngeal nerve (*small black arrows* in *C–E*) is visualized in the recess for the glossopharyngeal nerve (*white dotted arrow* in *C* and *D*). Just inferior to the glossopharyngeal nerve, there is a dural ring seen as slightly dark signal intensity at the apex of the JF (*white crossed arrow* in E). *F* and *G,* Just below the level of the dural ring, the recess for the CN X/XI complex (*white arrowhead*) and the vagus nerve (*black arrowhead*) is visualized. *H,* The spinal accessory nerve (*black arrow*) is visualized in the recess for the CN X/XI complex (*white arrowhead*) at the level of the lower end of the JF.

JF, with an emphasis on its nerve contents, the CSF recess adjacent to the JF can be partitioned into 3 parts craniocaudally: the recess for the cochlear aqueduct, the recess for the glossopharyngeal nerve, and the recess for the vagus nerve and accessory nerve.[2,8]

By using a different angle and different length for each CSF recess adjacent to the JF to the posterior petrous bone, we could easily differentiate each CSF recess. The cochlear aqueduct is a bony canal that encloses the perilymphatic duct connecting the subarachnoid space and the basal turn of the cochlea.[1] The cochlear aqueduct usually courses superiorly from the JF, sometimes has an opening at the superior part of the JF, and is very close to the recess for the glossopharyngeal nerve.[1] During microsurgery, the cochlear aqueduct provides a landmark on the subarachnoid side of the glossopharyngeal nerve in the JF.[8,15] However, because of the close proximity, the re-

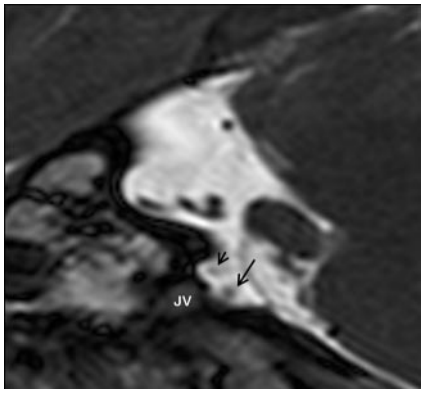

Fig 4. Oblique sagittal reformatted 3D-bFFE image at the level of the JF. The short arrow indicates the glossopharyngeal nerve within the recess for CN IX, and the long arrow indicates the vagus/spinal accessory nerve complex within the recess for the CN X/XI complex. JV indicates jugular vein.

cess for the cochlear aqueduct and the recess for the glossopharyngeal nerve can be mistaken for each other as seen on axial images, especially with the use of thicker sections.[1,2] Our results showed that the recess for the cochlear aqueduct has the most acute angle in relation to the posterior petrosal surface, consistently being $<50°$.

We found that the glossopharyngeal nerve ran parallel to the glossopharyngeal recess, which was at a broader angle to the posterior surface of the petrous bone than the recess for the cochlear aqueduct. Furthermore, the glossopharyngeal recess was shorter (shallower) than the recess for the cochlear aqueduct. In our study, the glossopharyngeal recess could, therefore, be well separated from the recess for the cochlear aqueduct by its angle and length. Given these findings, we suggest that identification of the recess for the cochlear aqueduct as seen on serial axial images can facilitate the localization of the glossopharyngeal recess and its nerve (glossopharyngeal nerve).

Among the 3 CSF recesses adjacent to the JF, the recess for CN X/XI demonstrated the broadest angle relative to the posterior petrosal surface. In addition, the recess for CN X/XI is the shallowest among the 3 CSF recesses. Identification of the recess for CN X/XI may also help to localize the corresponding nerves in the cisternal space and within the recess itself as seen on serial axial images.

The glossopharyngeal nerve is separated from the vagus and the accessory nerves by a dural septum, which is consistently observed ranging in width from 0.5 to 4.9 mm.[11,16-20] CN IX nerve is located anterosuperomedial to CN X and CN XI.[2] This dural septum was observed as a mild hypointensity just superior to the level of the vagus nerve between the recess for CN IX and the recess for CN X and CN XI in our study. However, the partial volume artifacts and unavoidable susceptibility artifacts due to the presence of an adjacent bony interface prevented the imaging from consistently identifying this dural structure.

At and near the JF, visualization of the cisternal segments of CN IX and the CN X/XI complex on 3D-bFFE was usually excellent in our study. A small fraction of the cases showed a poor result, which might be mostly due to banding artifacts induced by the strong magnetic susceptibility effect.[9,21] In contrast to axial scans, separability of the CN X/XI complex on oblique sagittal and coronal reformatted images was not adequate.

In previous radio-anatomic studies, CN X and CN XI were found to be placed anteromedially and adjacent to the internal jugular vein at the JF.[1,2] The vagus nerve courses together with the accessory nerves into the foramen. The nerves pass through the dura just inferior and slightly posterior to the glossopharyngeal nerve.[1] A previous CT study could not demonstrate separation of the vagus nerve from the accessory nerves at and near the JF.[1] The vagus nerve and accessory nerves enter the foramen together or nearly together, passing through the dura inferior and slightly posterior to the glossopharyngeal nerve.[1,2,11] Although CT could not demonstrate the vagus and accessory nerves as 2 separate nerves,[1] the nerves were usually found to be separated by less than a few millimeters at the entrance to the foramen in microsurgical anatomy.[1,11,18]

In contrast to a previous CT study, recent high-resolution MR imaging studies have shown that the vagus nerve is separated from the accessory nerve within the cisternal spaces. However, the 2 nerves were shown to intermingle with each other within the JF.[5,7]

From our results showing poor separability of the CN X/XI complex within the cisternal space, we speculate that the rather oblique course and close proximity of the accessory nerves to the vagus nerve are responsible for the inseparability seen on axial images and on oblique sagittal and coronal reformatted images.[1] The anatomy of the accessory nerves near the dural orifice in close proximity to the vagus nerve may be another factor for the inseparability from the vagus nerve.[11] A limitation of modest spatial resolution in 3D-bFFE images applied in our study might also contribute to the inseparability of the nerves.

This study has some limitations. Although 3D-bFFE with a magnetic field strength of 1.5T provides quite good resolution and image quality, a higher resolution image with a higher magnetic strength may be better for the identification of microstructures such as the lower cranial nerves.[7] Second, we did not consider the entire course of the lower cranial nerves, which might be clinically more important. Therefore, we did not study intraforaminal structures, such as the intraforaminal nerves, the internal jugular vein, the inferior petrosal vein, and the posterior meningeal artery, which might traverse the JF and hinder the visualization of the lower cranial nerves. To distinguish these microvascular structures from the lower cranial nerves, a contrast-enhanced study might be helpful.[5,7]

Identification and better knowledge of the lower cranial nerves that pass through the cistern and foramen enable a better understanding and allow identification of the complex anatomy and pathologic process as well.[22] As indicated in previous studies,[1,11,22] the variability of the nerve course may prevent the identification of the lower cranial nerves with precision. However, knowledge of the relationship of the lower cranial nerves to a rather fixed structure such as the CSF recesses adjacent to the JF and posterior petrosal surface might give new insights into the evaluation of the cisternal segments of the lower cranial nerves.

Conclusions

Use of the angles of each CSF recess adjacent to the JF may be helpful in identification of each cisternal segment of the lower cranial nerves in 3D-bFFE imaging. The cisternal segments of CN IX, CN X, CN XI, and the 3 parts of the CSF recess adjacent to the JF can be easily and clearly visualized by the use of 3D-bFFE MR imaging techniques.

References

1. Rubinstein D, Burton BS, Walker AL. **The anatomy of the inferior petrosal sinus, glossopharyngeal nerve, vagus nerve, and accessory nerve in the jugular foramen.** *AJNR Am J Neuroradiol* 1995;16:185–94
2. Tekdemir I, Tuccar E, Aslan A, et al. **The jugular foramen: a comparative radioanatomic study.** *Surg Neurol* 1998;50:557–62
3. Seitz J, Held P, Frund R, et al. **Visualization of the IXth to XIIth cranial nerves using 3-dimensional constructive interference in steady state, 3-dimensional magnetization-prepared rapid gradient echo and T2-weighted 2-dimensional turbo spin echo magnetic resonance imaging sequences.** *J Neuroimaging* 2001;11:160–64
4. Suzuki H, Maki H, Maeda M, et al. **Visualization of the intracisternal angioarchitecture at the posterior fossa by use of image fusion.** *Neurosurgery* 2005;56:335–42
5. Davagnanam I, Chavda SV. **Identification of the normal jugular foramen and lower cranial nerve anatomy: contrast-enhanced 3D fast imaging employing steady-state acquisition MR imaging.** *AJNR Am J Neuroradiol* 2008;29:574–76
6. Casselman J, Mermuys K, Delanote J, et al. **MRI of the cranial nerves: more than meets the eye—technical considerations and advanced anatomy.** *Neuroimaging Clin N Am* 2008;18:197–231
7. Linn J, Peters F, Moriggl B, et al. **The jugular foramen: imaging strategy and detailed anatomy at 3T**. *AJNR Am J Neuroradiol* 2009;30:34–41. Epub 2008 Oct 2
8. Ozveren MF, Ture U, Ozek MM, et al. **Anatomic landmarks of the glossopharyngeal nerve: a microsurgical anatomic study.** *Neurosurgery* 2003;52:1400–10
9. Jung NY, Moon WJ, Lee MH, et al. **Magnetic resonance cisternography: comparison between 3-dimensional driven equilibrium with sensitivity encoding and 3-dimensional balanced fast-field echo sequences with sensitivity encoding.** *J Comput Assist Tomogr* 2007;31:588–91
10. Tsuchiya K, Aoki C, Hachiya J. **Evaluation of MR cisternography of the cerebellopontine angle using a balanced fast-field-echo sequence: preliminary findings**. *Eur Radiol* 2004;14:239–42
11. Rhoton AL. **Jugular foramen.** *Neurosurgery* 2000;47(suppl 3):267–85
12. Shapiro R. **Compartmentation of the jugular foramen.** *J Neurosurg* 1972;36:340–43
13. Dodo Y. **Observations on the bony bridging of the jugular foramen in man.** *J Anat* 1986;144:153–65
14. Sturrock RR. **Variations in the structure of the jugular foramen of the human skull.** *J Anat* 1988;160:227–30
15. Rutka J, Nedzelski J. **Translabyrinthine identification of the cochlear aqueduct: a helpful landmark during inferomedial temporal bone dissection.** *J Otolaryngol* 1991;20:184–87
16. Ayeni SA, Ohata K, Tanaka K, et al. **The microsurgical anatomy of the jugular foramen.** *J Neurosurg* 1995;83:903–09
17. Kveton JF, Cooper MH. **Microsurgical anatomy of the jugular foramen region.** *Am J Otol* 1988;9:109–12
18. Lang J. **Anatomy of the brainstem and the lower cranial nerves, vessels, and surrounding structures.** *Am J Otol* 1985;(suppl):1–19
19. Saleh E, Naguib M, Aristegui M, et al. **Lower skull base: anatomic study with surgical implications.** *Ann Otol Rhinol Laryngol* 1995;104:57–61
20. Katsuta T, Rhoton AL, Matsushima T. **The jugular foramen: microsurgical anatomy and operative approaches.** *Neurosurgery* 1997;41:149–201
21. Lane JI, Ward H, Witte RJ, et al. **3-T imaging of the cochlear nerve and labyrinth in cochlear-implant candidates: 3D fast recovery fast spin-echo versus 3D constructive interference in the steady state techniques.** *AJNR Am J Neuroradiol* 2004;25:618–22
22. Lustig LR, Jackler RK. **The variable relationship between the lower cranial nerves and jugular foramen tumors: implications for neural preservation.** *Am J Otol* 1996;17:658–68